

# Synthetic Antiferromagnets with Steplike Hysteresis Loops and High- $T_C$ Based on All-Perovskite $\text{La}_{0.7}\text{Sr}_{0.3}\text{MnO}_3$ Superlattices

Haoran Xu,<sup>1,2</sup> Feng Chen,<sup>1,\*</sup> Binbin Chen,<sup>2</sup> Feng Jin,<sup>1,2</sup> Chao Ma,<sup>2</sup> Liqiang Xu,<sup>2</sup> Zhuang Guo,<sup>2</sup> Lili Qu,<sup>2</sup> Da Lan,<sup>2</sup> and Wenbin Wu<sup>1,2</sup>

<sup>1</sup>*Anhui Province Key Laboratory of Condensed Matter Physics at Extreme Conditions, High Magnetic Field Laboratory, Chinese Academy of Sciences, Hefei 230031, China*

<sup>2</sup>*Hefei National Laboratory for Physical Sciences at Microscale, University of Science and Technology of China, Hefei 230026, China*



(Received 4 February 2018; revised manuscript received 27 April 2018; published 23 August 2018)

Synthetic antiferromagnets with high Curie temperature (approximately 290 K) are realized among all-perovskite  $\text{La}_{0.7}\text{Sr}_{0.3}\text{MnO}_3$  (LSMO)/ $\text{CaRu}_{0.5}\text{Ti}_{0.5}\text{O}_3$  (CRTO) superlattices, which show antiferromagnetic (AF) interlayer exchange coupling (IEC) rather than traditional interfacial exchange coupling that is usually observed under the Curie temperature of the spacer. The system shows layer-resolved magnetic switching, resulting in sharp steplike hysteresis loops with magnetization plateaus depending on the repetition number of the stacking bilayers. This bilinear IEC can be easily changed to biquadratic IEC by change of orthorhombic  $\text{NdGaO}_3(001)$  substrate to cubic  $(\text{LaAlO}_3)_{0.3}(\text{SrAl}_{0.5}\text{Ta}_{0.5}\text{O}_3)_{0.7}(001)$  substrate. The strength of AF IEC increases with decrease of temperature, and the modeling results suggest that both magnetic LSMO and the CRTO space layer play a role in this behavior. Remarkably, the LSMO/CRTO system shows controllability of AF-IEC behavior under a moderate magnetic field of hundreds of oersteds. These observations may have potential applications in future oxide spintronic devices.

DOI: 10.1103/PhysRevApplied.10.024035

## I. INTRODUCTION

Antiferromagnets (AFMs) have been used as pinning layers in spin valves and magnetic tunnel junctions in magnetic devices in recent decades [1]. Their inert reaction to a disturbing magnetic field and lack of stray fields make them more suitable for high-density storage compared with ferromagnets, and innovative concepts of memory devices directly based on AFMs were developed recently [2]. For bulk AFMs, very large external fields are needed to induce spin-flop transitions, resulting in their being difficult to study experimentally. Because of advances in atomic-level control in thin-film deposition, ferromagnetic (FM) layers periodically interleaved with nonmagnetic spacers can be constructed as synthetic AFMs, where the adjacent FM layers exhibit alternate magnetization due to antiferromagnetic (AF) interlayer exchange coupling (IEC) [3–5]. The properties of these synthetic AFMs can be easily tuned by moderate magnetic fields [4,6]. For example, the hysteresis loops of the Fe/Cr/Fe system [7] and the [(Co/Pt)/Co/Ru] system [8] show metamagnetic transitions with only a few hundred or thousand gauss. Moreover, they all show a layer-resolved magnetic switching with step-like transitions, which is closely related to the behavior of individual FM layers and is important for modern magnetic

technology, such as perpendicular recording for higher data storage density, where local behaviors are crucial.

The IEC of synthetic AFMs with metallic spacers is different from that of those with insulating spacers; that is, the IEC oscillates between FM and AF types as a function of spacer thickness for the former [9–11], while the IEC strength decays monotonically with the spacer thickness for the latter [12,13]. The IEC strength also shows a temperature dependency, but the dominant mechanism is still unclear [14–16]. To explain these behaviors, many theories, such as the Ruderman-Kittel-Kasuya-Yosida model, the free-electron model, the one-band tight-binding model, the *s-d* mixing model, and the quantum interference model, have been proposed [9,17–20]. So far, most of the theoretical and experimental achievements made on AF IEC are built on magnetic multilayers with transition metals or alloys. It is noted that there is an interesting AF-exchange-coupling work on topological-insulator-based heterostructures [21]. However, AF IEC remains rare and challenging among all-perovskite oxide multilayers. Perovskite oxides have displayed a diverse array of functional and emergent properties due to the strong correlations between charge, spin, lattice, and orbital degrees of freedom. Therefore, realizing synthetic AFMs among all-perovskite oxides may open new pathways for device applications.

Recently, we realized synthetic AFMs and controllable AF-IEC behavior with  $\text{La}_{0.67}\text{Ca}_{0.33}\text{MnO}_3$  (LCMO)/

\*fchen@hmfl.ac.cn

$\text{CaRu}_{0.5}\text{Ti}_{0.5}\text{O}_3$  (CRTO) superlattices [22]. To achieve these results, epitaxial growth with atomic-layer control, ultrathin FM layers with ferromagnetism retained at nanoscale thickness, and robust in-plane uniaxial magnetic anisotropy are required at the same time. LCMO/CRTO superlattices display a Curie temperature ( $T_C$ ) of between approximately 140 K and approximately 230 K, depending on their configurations, which is much lower than room temperature (RT).  $\text{La}_{0.7}\text{Sr}_{0.3}\text{MnO}_3$  (LSMO) could be a suitable substitute for LCMO, since bulk LSMO is a half-metallic ferromagnet and has  $T_C$  of around 370 K [23].  $T_C$  is enhanced in LSMO/ $\text{SrRu}_{1-x}\text{Ti}_x\text{O}_3$  combinations, but pure bilinear AF IEC cannot be obtained even by changing the composition and the thickness of the  $\text{SrRu}_{1-x}\text{Ti}_x\text{O}_3$  spacer [24]. In this work, we build synthetic all-perovskite oxide superlattices composed of ultrathin LSMO layers and CRTO spacers, which substantially increases  $T_C$  of the system to approximately 290 K. LSMO/CRTO superlattices demonstrate not only a clear bilinear AF-IEC behavior but also layer-resolved magnetic switching with a series of magnetization plateaus depending on the repetition number of the stacking bilayers. The AF IEC in the LSMO/CRTO system is strongly correlated with the symmetry mismatch, and its strength increases when the temperature is decreased.

## II. MATERIAL GROWTH AND CHARACTERIZATION

The LSMO/CRTO superlattices are grown on (001)-oriented  $\text{NdGaO}_3$  (NGO;  $Pbnm$  symmetry) and  $(\text{LaAlO}_3)_{0.3}(\text{SrAl}_{0.5}\text{Ta}_{0.5}\text{O}_3)_{0.7}$  (LSAT;  $Pm\bar{3}m$  symmetry) substrates by pulsed-laser deposition. The ceramic targets of LSMO and CRTO are prepared by standard solid-state reactions. The 248-nm ultraviolet radiation from a KrF excimer laser is used with a frequency of 5 Hz and a laser energy density of 2.0 J/cm<sup>2</sup>. The growth oxygen pressure is 30 Pa, and the substrate temperature is kept at 700 °C. After the deposition, the samples are annealed *in situ* for 15 min and then cooled to RT under an oxygen pressure of 10<sup>3</sup> Pa.

The superlattice structures are characterized by high-resolution X-ray diffraction using Cu  $K\alpha_1$  radiation ( $\lambda = 1.5406 \text{ \AA}$ ) and scanning transmission electron microscopy (STEM). The magnetization is measured with a Quantum Design vibrating sample magnetometer with an applied magnetic field ( $H$ ) along the in-plane [010] direction (orthorhombic index for NGO and cubic index for LSAT; see the Supplemental Material [45]).

## III. RESULTS AND DISCUSSION

To maintain the internal LSMO layers in identical interfacial arrangements, all superlattices are initiated with CRTO and terminated with a CRTO layer. For clarity, the

sample is written as  $[x/y]_N$  (where  $x$  and  $y$  denote the thicknesses of LSMO and CRTO in nanometers, respectively, and  $N$  denotes the period). The results for representative  $[2.8/1.2]_{10}$  grown on NGO are presented in Fig. 1. The high-resolution X-ray  $\theta$ -2 $\theta$  linear scan displays clear Laue fringes and first-order satellite peaks ( $-1, +1$ ) around the main reflection (0), as observed in Fig. 1(a), indicating a smooth surface and clear interfaces as well. The high quality of  $[2.8/1.2]_{10}$  is confirmed by reciprocal-space mapping [Fig. 1(b)], where very confined reflections are observed. Cross-section STEM images with elemental mapping measured by spatially resolved electron-energy-loss spectroscopy (EELS) show element-resolved interfaces between LSMO and CRTO layers [Figs. 1(c) and S1] [45]. The period thickness obtained from the X-ray  $\theta$ -2 $\theta$  linear scan and STEM images is consistent with the nominal thickness. The LSMO layer is fixed at a thickness of 2.8 nm (approximately seven unit cells) to avoid the effects of the so-called dead layer [25–28], which will decrease  $T_C$  of manganite films. In LSMO/ $\text{SrRuO}_3$  superlattices [28,29], LSMO layers with a thickness of two unit cells show a stabilized FM order due to the charge-transfer mechanism. Figure 1(d) shows that 2.8-nm thickness is sufficient to retain the ferromagnetism of the LSMO layer.

The CRTO spacer is derived from paramagnetic  $\text{CaRuO}_3$  by doping with Ti, which has weak ferromagnetism below 38 K and semiconductorlike behavior [30]. The NGO substrate shows paramagnetic behavior, and the normalized  $M$ - $T$  curve of the superlattice exhibits  $T_C$  of approximately 290 K, as illustrated in Fig. 1(d). A sudden drop of the magnetization appears at about 215 K in the  $M$ - $T$  curve (indicated by the black arrow), and then the curve overlaps with the paramagnetic signal of NGO at low temperature. Similar  $M$ - $T$  curves have been observed in LCMO/CRTO and LSMO/ $\text{SrRu}_{1-x}\text{Ti}_x\text{O}_3$  systems [22,24]. Both AF IEC and AF interfacial exchange coupling can result in the reduction of magnetization. AF interfacial exchange coupling is usually observed below  $T_C$  of the spacer, as in the LSMO/ $\text{SrRuO}_3$  system [28,31]. In contrast, here the LSMO/CRTO  $[2.8/1.2]_{10}$  system shows a drop of magnetization around 215 K, which is obviously far above 38 K. This means when the AF coupling appears in the LSMO/CRTO system, the CRTO has not changed to a ferromagnet yet. The result implies that LSMO/CRTO has AF-IEC behavior rather than AF-interfacial-exchange-coupling behavior. To clarify this point, we also measure the magnetic hysteresis loops ( $M$ - $H$  curves) of the superlattice at 200 K [Fig. 1(e)], where the paramagnetic signal of NGO is subtracted. Four steplike metamagnetic transitions appear as indicated by blue arrows, and the remnant magnetization  $M_R$  is nearly zero. These are significant traits of bilinear Heisenberg-like AF IEC due to the switching of LSMO in a certain sequence [32].

The AF IEC is further explored among LSMO/CRTO superlattices of the form  $[2.8/1.2]_N$  with different period

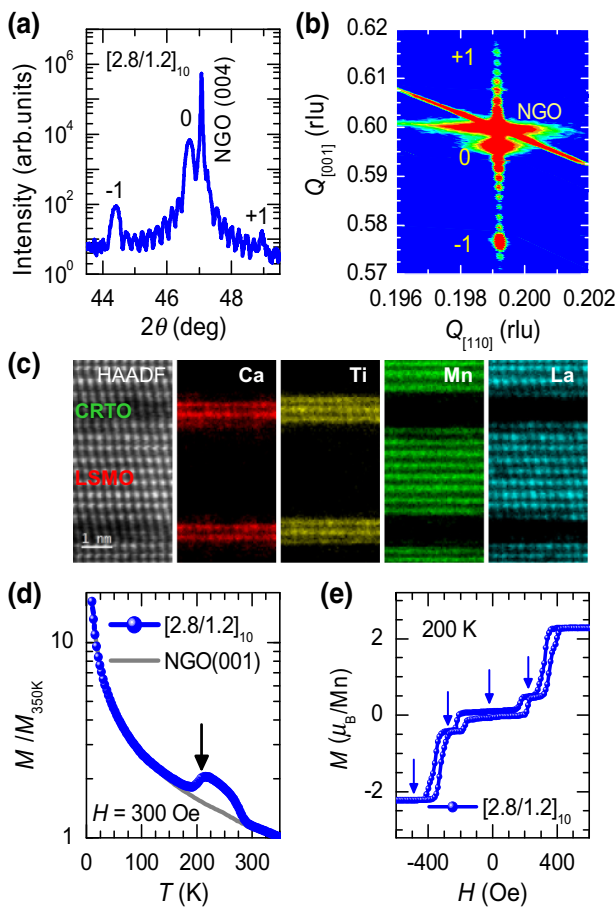


FIG. 1. Characterization of LSMO/CRTO superlattice,  $[2.8/1.2]_{10}$ , grown on NGO(001). (a) High-resolution X-ray  $\theta$ - $2\theta$  linear scan. (b) Off-specular reciprocal-space mapping on the (116) main reflection, where the main reflection (116) (denoted as “0”) and the satellites (denoted as “ $\pm 1$ ”) are narrow in  $Q_{[110]}$  direction and sharply defined even with the thickness fringes. Note that  $Q_{[110]}$  and  $Q_{[001]}$  are coordinates in the reciprocal space and for the present system they are along the in-plane and out-of-plane direction in real space, respectively. The in-plane (out-of-plane) lattice constant can be calculated as  $\lambda/Q_{[110]} (3\lambda/Q_{[001]})$ . (c) Cross-section high-angle annular dark-field (HAADF) STEM image with elemental mapping measured by spatially resolved EELS. (d) Temperature-dependent magnetization curve. The magnetization is normalized to the value at 350 K, and the paramagnetic signal of the bare NGO(001) substrate is included for comparison. (e) The corresponding field-dependent magnetization loops measured at 200 K. rlu.

$N$ . The normalized  $M$ - $T$  curves show nearly the same  $T_C$  of approximately 290 K and an obvious reduction in magnetization around approximately 215 K, as shown in Fig. 2. All  $M$ - $H$  curves present steplike metamagnetic transitions (Fig. 3), which means the realization of AF IEC in the LSMO/CRTO system is feasible and it is independent on the periods. The red  $M$ - $H$  curves indicate sweep along decreasing field and the blue curves indicate sweep along increasing field. The right panel shows the switching

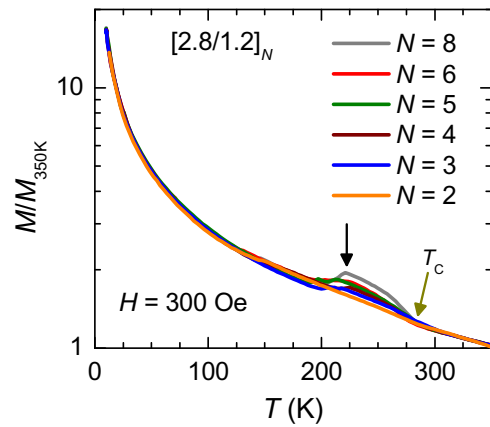


FIG. 2. Temperature-dependent magnetizations of LSMO/CRTO superlattices,  $[2.8/1.2]_N$ , grown on NGO(001) are normalized to the value at 350 K. The black arrow denotes the reduction in magnetization.

process in the decreasing field direction. To facilitate analysis, four dashed lines are symmetrically and equidistantly distributed as guidelines, and they are numbered as  $-2$ nd,  $-1$ st,  $1$ st, and  $2$ nd from left to right. The LSMO layer near the substrate is defined as layer 1 for convenience in the following discussion. For  $N=2$ , the  $M$ - $H$  loop has two abrupt steps, corresponding to the antiparallel and parallel alignments of LSMO layers. The small  $M_R$  could be attributed to the sample quality, where the thickness of two LSMO layers might have a small deviation, resulting in a nonzero  $M_R$  for antiparallel alignment. For  $N=3$ , the loops centered around the  $-2$ nd and  $2$ nd lines are attributed to the switching of the central LSMO layer, which interacts with two outer LSMO layers (layers 1 and 3). To overcome the interaction, twice as much energy as for  $N=2$  is needed. The  $M_R \approx (1/3)M_S$  ( $M_S$  is the saturated magnetic moment) at step 1 originates from the single uncompensated LSMO layer in the AF state. For  $N=4$ , four steps are displayed in the  $M$ - $H$  curve, and the loops are centered around the  $-2$ nd,  $-1$ st,  $1$ st, and  $2$ nd lines, respectively. This means that the internal LSMO layers reverse first at higher field because of the twice as much energy needed for internal FM layers. Given that internal layers 2 and 3 are in an identical exchange environment, two possible switching sequences can be adopted from the positive to negative saturation: layers 2-4-1-3 or layers 3-1-4-2. The schematic in Fig. 3 shows only the former.

For a larger even  $N$ , these two sequences are also applicable. On account of the magnitude of the magnetic moment at step 1 [approximately  $(1/3)M_S$  and approximately  $(1/4)M_S$ ] for  $N=6$  and  $8$ , several internal LSMO layers reverse at the same time. The switching sequences should be (2,4)-6-1-(3,5) or the reverse, and (2,4,6)-8-1-(3,5,7) or the reverse, respectively. For odd  $N=5$ , the hysteresis loop differs dramatically from that for even  $N$ . As  $H$  decreases, considering the magnetic moment  $M \approx (3/5)M_S$

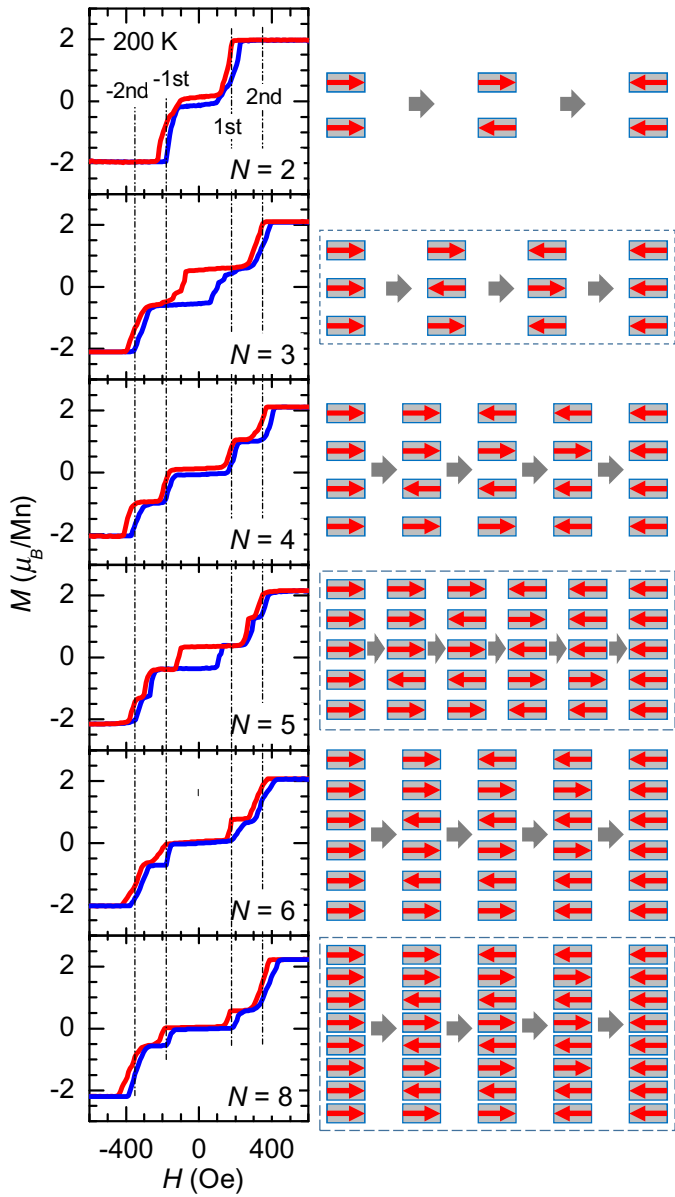


FIG. 3. Field-dependent magnetization loops of LSMO/CRT superlattices,  $[2.8/1.2]_N$ , grown on NGO(001) measured at 200 K. The right panel shows the switching process of LSMO layers in decreasing field direction and the red arrows represent the direction of magnetization of individual LSMO layers.

at step 1, we think layer 2 (or layer 4) switches to the opposite direction first, and then layer 4 (or layer 2) switches at step 2, bringing all layers into the AF array with nonzero  $M_R \approx (1/5)M_S$  for one uncompensated LSMO layer. Layers 1, 3, and 5 and layers 2 and 4 switch simultaneously at step 3, and layers 2 and 4 reverse in sequence at steps 4 and 5, respectively. These results match quite well with Monte Carlo simulations for the prototype AF system [32], although inverted steps have not been observed for  $N = 5$ .

LSMO/CRT superlattices of the form  $[2.8/1.2]_N$  have also been grown on cubic LSAT(001) substrates, which

means the in-plane strain is isotropic. Figure 4(a) shows that the samples have  $T_C$  of around 300 K and exhibit a peak in magnetization as the temperature decreases to approximately 250 K, and then the magnetization reduces as the temperature decreases from approximately 250 K to approximately 150 K. The reductions of magnetization are similar to those of samples grown on NGO(001), where the reductions look sharper and start at around 215 K (Fig. 2). This implies the potential existence of AF IEC in LSMO/CRT grown on LSAT. The  $M$ - $H$  curves measured at 150 K [Fig. 4(b)] are far from showing abrupt steplike metamagnetic transitions, and these loops with nonzero  $M_R$  are centered at the origin. These distinctly different  $M$ - $H$  curves may stem from the biquadratic IEC ( $90^\circ$  coupling) on LSAT(001) rather than bilinear Heisenberg-like IEC on NGO(001) [33–35]. The transitions indicated by black arrows in Fig. 4(b) are at approximately  $(1/2)M_S$ , which is strong evidence for the biquadratic AF IEC [35]. The lattice constants of NGO and cubic LSAT differ only slightly, but their structural symmetries are orthorhombic and cubic, respectively. Structural symmetry mismatch between components has a great impact on the crystal quality and magnetic properties of samples [36,37], and the roughness at the interfaces can result in competition between FM and AF states and ultimately result in biquadratic IEC [38]. The structural characterization by high-resolution X-ray  $\theta$ - $2\theta$  linear scan evinces relatively good crystal quality of the sample grown on LSAT(001) [Fig. 4(c)]. Thus, the effects of the roughness at interfaces might be excluded. The biquadratic IEC could be attributed to the domain structure, since cubic LSAT can cause the formation of  $90^\circ$  domain ordering in rhombohedral LSMO due to the shear-strain relaxation [39]. To maintain the lowest domain wall energy, the couplings between FM layers tend to be biquadratic IEC. Anyway, the LSMO/CRT superlattices also show AF-IEC behavior on LSAT substrates, but without pure bilinear IEC and layer-resolved magnetic switching. Except for the symmetry mismatch, the  $M$ - $H$  curves observed for LSMO/CRT superlattices,  $[x/y]_{10}$ , suggest the thickness variation of LSMO and CRT also has great effects on the AF-IEC behavior (see Fig. S2) [45].

The effective IEC strength should be temperature dependent, as proved by FM-resonance measurements on Fe/Pd/Fe trilayers [40], where the coupling strength at 77 K is nearly twice as large as that at RT. Therefore,  $M$ - $H$  curves of the superlattice  $[2.8/1.2]_{10}$  grown on NGO(001) are measured at different temperatures (50–280 K), as shown in Fig. 5(a). Apparent AF-IEC characteristics can be observed from 50 to 270 K. Here we extract the value of the field where it begins to drop at each step in decreasing field direction from the  $M$ - $H$  curves to delineate the phase diagram, as shown in Fig. 5(b). With decrease of the field there exists an intermediate state (IS) before the system evolves to the AF state, and the magnetization

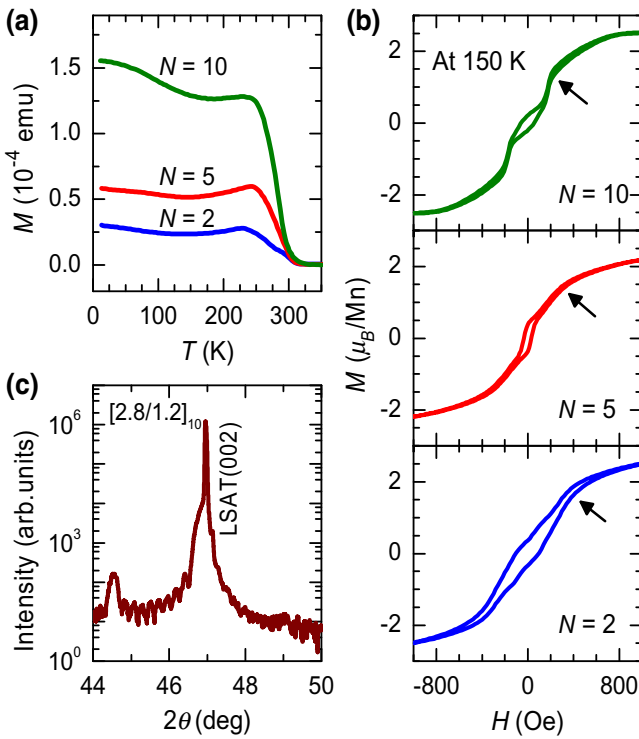


FIG. 4. (a) Temperature-dependent magnetization curves of LSMO/CRTO superlattices,  $[2.8/1.2]_N$ , grown on LSAT(001) measured at 300 Oe. (b) The corresponding field-dependent magnetization loops measured at 150 K. (c) High-resolution X-ray  $\theta$ - $2\theta$  linear scan for  $[2.8/1.2]_{10}$  grown on LSAT(001).

configuration can be softly modulated merely by hundreds of gauss in a wide temperature region. Also, it is clear that the lower the temperature, the broader the region of the AF state. This is different from the LCMO/CRTO system, where the AF state and the IS have a crossover when the temperature is lower than 50 K [22], which means that in the LSMO/CRTO system the IEC is still stronger than the magnetic anisotropic energy even at low temperature.

The IEC strength of the system is given by the following relationship:

$$J_{IEC} = -H_S M_S t_{FM} / 2\alpha,$$

where  $H_S$ ,  $M_S$ , and  $t_{FM}$  are the saturation field, saturation magnetization, and thickness of the LSMO layer, respectively.  $\alpha$  ranges from 1 in a simple sandwich structure to 2 as the number of magnetic layer becomes very large [5]. With this formula, the IEC strength of  $[2.8/1.2]_{10}$  can be evaluated as a function of temperature by extraction of the parameters from the corresponding  $M$ - $H$  curves, as shown in Figs. 5(c)–5(e) (blue spheres).  $J_{IEC}$  increases monotonously with decreasing temperature, demonstrating a strong temperature-dependent behavior.

In principle, two prevailing models have been discussed in the literature to explain the temperature dependence of

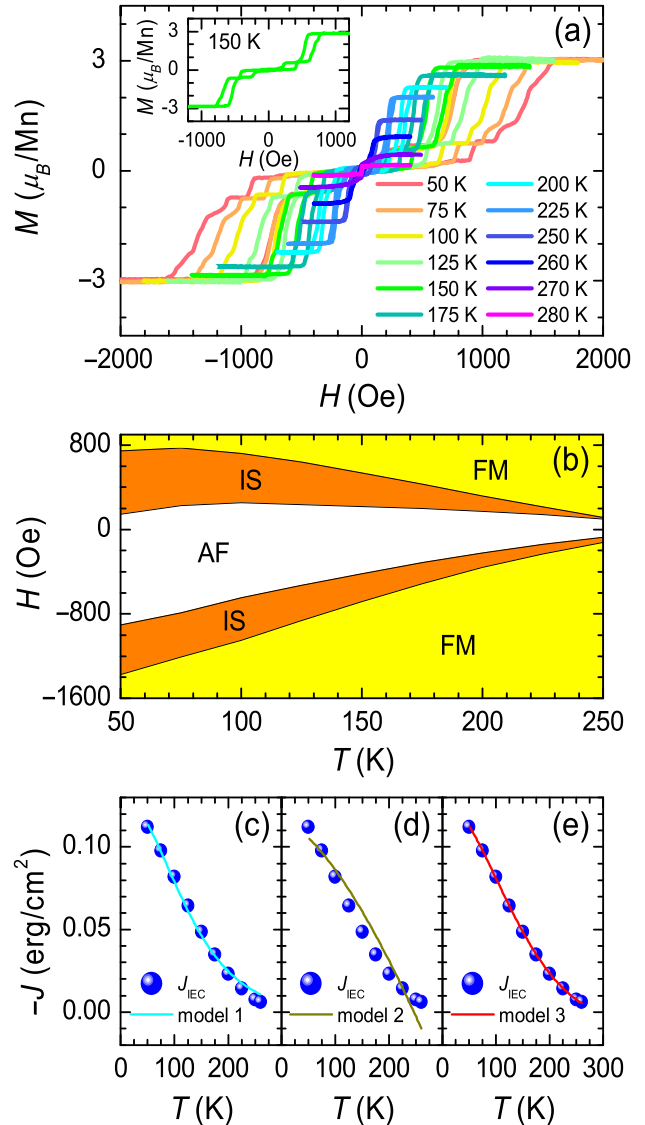


FIG. 5. (a) Field-dependent magnetization loops of LSMO/CRTO superlattices,  $[2.8/1.2]_{10}$ , grown on NGO(001) measured at different temperatures. The inset shows the complete loop measured at 150 K. (b) Phase diagram drawn with the values of the field where magnetization begins to drop at each step in the decreasing field direction of loops measured at different temperatures. FM denotes that all LSMO layers are parallel, AF denotes that all adjacent LSMO layers are antiparallel, and IS denotes that two LSMO layers are parallel and the rest of eight LSMO layers are antiparallel. Temperature-dependent IEC strength ( $J_{IEC}$ , blue spheres) and the fitting results obtained with (c) model 1, (d) model 2, and (e) model 3.

IEC strength [15,16,41]. In model 1, the temperature effect is related to the Fermi surface of the spacer material, where the temperature variations of the IEC are provided by the fact that electrons within the spacer layer have to follow Fermi-Dirac statistics. The velocity of carriers at the stationary points of the spacer Fermi surface governs the

temperature dependence. The expression in model 1 is as follows:

$$J_{IEC,1} = J_0[(T/T_0)/\sinh(T/T_0)],$$

where  $T_0 = v_F/2\pi k_B d$  is the characteristic temperature,  $v_F$  is the Fermi velocity, and  $d$  is the thickness of the spacer. In model 2, the magnetic excitations of thermal spin waves in coupled FM films with relatively low  $T_C$  drive the temperature dependence of IEC. This is given as

$$J_{IEC,2} = J_0[1 - (T/T_C)^{3/2}],$$

where  $T_C$  is the Curie temperature of the system (not that of the bulk). Note that  $J_0$  is a constant and is different in these two formulas. The results are fitted by model 1 [Fig. 5(c)] and model 2 [Fig. 5(d)]. It is seen that the fitting result obtained with model 1 is more rational, but there still exists an obvious deviation when the temperature is higher than 200 K. Thus, the data are further fitted by a revised model [model 3; Fig. 5(e)], which combines models 1 and 2 as suggested by Almeida *et al.* [42]; that is,  $J_{IEC,3} = J_{IEC,1} \times J_{IEC,2}$ . Clearly, the results are best fitted by this model, which leads to  $T_C$  of 292 K. This is almost the same as we obtained from the  $M$ - $T$  curves [Fig. 1(d)]. Although  $v_F \approx 8.1 \times 10^6$  cm/s, derived from  $T_0 \approx 83$  K obtained from this fitting, is 1 or 2 orders of magnitude smaller than that of Ru and Sr<sub>2</sub>RuO<sub>4</sub> [43], it is comparable with that of Ca<sub>3</sub>Ru<sub>2</sub>O<sub>7</sub> [44], which behaves like a semiconductor as well. Therefore, the best fitting by model 3 implies that the CRTO spacer with low carrier density and FM layers of the system with  $T_C$  near RT both play a role in the dependency of temperature and IEC strength.

The origin of the temperature dependence of IEC has been long debated. In quantum-well theory, it is suggested that the strong variation of the coupling with temperature depends not only on the spacer Fermi surface but also on the degree of confinement of magnetic carriers in the spacer quantum well [16]. In the Gd/Y/Tb system, Tb and Gd have  $T_C$  of 220 and 293 K, respectively. We believe that the difference in the reflection coefficient for electrons with opposite spins inside a quantum well, determined by the exchange splitting of the valence bands of the magnetic material, leads to polarization of the valence band of the spacer material, mediating magnetic coupling. When the temperature is closer to  $T_C$ , the IEC strength is increasingly lower [14]. In addition, an alternative explanation for the strong decrease of IEC strength with increasing temperature is a magnetically dead layer at the interfaces. The dead layer is expected to become thinner at lower temperature, and the quantum well is sharper than that at RT, which modifies the confinement of the carriers and thus leads to a strong temperature dependence of IEC [16].

#### IV. CONCLUSIONS

In conclusion, synthetic AFMs with high  $T_C$  and bilinear AF IEC are realized in all-perovskite LSMO/CRTO superlattices. Steplike metamagnetic transitions depending on the repetition number of bilayers are clearly seen due to the separate switching of the outer and internal LSMO layers. Cubic anisotropy introduced by the substrate could lead to biquadratic IEC instead of bilinear IEC. The fitting results suggest that both the spacers and the FM layers play a role in the temperature dependence of IEC strength.

#### ACKNOWLEDGMENTS

This work was supported by the National Key Research and Development Program of China (Grants No. 2016YFA0401003 and No. 2017YFA0403502) and the National Natural Science Foundation of China (Grants No. 11474263, No. 11574324, No. 11574281, and No. U1432251).

- [1] S. A. Wolf, D. D. Awschalom, R. A. Buhrman, J. M. Daughton, S. von Molnár, M. L. Roukes, A. Y. Chtchelkina, and D. M. Treger, Spintronics: A spin-based electronics vision for the future, *Science* **294**, 1488 (2001).
- [2] T. Jungwirth, X. Martí, P. Wadley, and J. Wunderlich, Antiferromagnetic spintronics, *Nat. Nanotechnol.* **11**, 231 (2016).
- [3] C. F. Majkrzak, J. W. Cable, J. Kwo, M. Hong, D. B. McWhan, Y. Yafet, J. V. Waszczak, and C. Vettier, Observation of a Magnetic Antiphase Domain Structure with Long-Range Order in a Synthetic Gd-Y Superlattice, *Phys. Rev. Lett.* **56**, 2700 (1986).
- [4] S. S. P. Parkin, N. More, and K. P. Roche, Oscillations in Exchange Coupling and Magnetoresistance in Metallic Superlattice Structures: Co/Ru, Co/Cr, and Fe/Cr, *Phys. Rev. Lett.* **64**, 2304 (1990).
- [5] S. S. P. Parkin, Systematic Variation of the Strength and Oscillation Period of Indirect Magnetic Exchange Coupling Through the 3d, 4d, and 5d Transition Metals, *Phys. Rev. Lett.* **67**, 3598 (1991).
- [6] M. T. Johnson, S. T. Purcell, N. W. E. McGee, R. Coehoorn, J. aan de Stegge, and W. Hoving, Structural Dependence of the Oscillatory Exchange Interaction Across Cu Layers, *Phys. Rev. Lett.* **68**, 2688 (1992).
- [7] O. Hellwig, T. L. Kirk, J. B. Kortright, A. Berger, and E. E. Fullerton, A new phase diagram for layered antiferromagnetic films, *Nat. Mater.* **2**, 112 (2003).
- [8] A. Azevedo, C. Chesman, S. M. Rezende, F. M. de Aguiar, X. Bian, and S. S. P. Parkin, Biquadratic Exchange Coupling in Sputtered (100) Fe/Cr/Fe, *Phys. Rev. Lett.* **76**, 4837 (1996).
- [9] P. Bruno and C. Chappert, Oscillatory Coupling Between Ferromagnetic Layers Separated by a Nonmagnetic Metal Spacer, *Phys. Rev. Lett.* **67**, 1602 (1991).
- [10] M. D. Stiles, Exchange coupling in magnetic heterostructures, *Phys. Rev. B* **48**, 7238 (1993).

- [11] J. Unguris, R. J. Celotta, and D. T. Pierce, Observation of Two Different Oscillation Periods in the Exchange Coupling of Fe/Cr/Fe(100), *Phys. Rev. Lett.* **67**, 140 (1991).
- [12] J. Faure-Vincent, C. Tiusan, C. Bellouard, E. Popova, M. Hehn, F. Montaigne, and A. Schuhl, Interlayer Magnetic Coupling Interactions of Two Ferromagnetic Layers by Spin Polarized Tunneling, *Phys. Rev. Lett.* **89**, 107206 (2002).
- [13] J. C. Slonczewski, Conductance and exchange coupling of two ferromagnets separated by a tunneling barrier, *Phys. Rev. B* **39**, 6995 (1989).
- [14] K. M. Döbrich, M. Wietstruk, J. E. Prieto, F. Heigl, O. Krupin, K. Starke, and G. Kaindl, Temperature-Induced Reversal of Magnetic Interlayer Exchange Coupling, *Phys. Rev. Lett.* **100**, 227203 (2008).
- [15] J. Lindner, C. Rüdt, E. Kosubek, P. Poulopoulos, K. Baberschke, P. Blomquist, R. Wäppling, and D. L. Mills,  $T^{3/2}$  Dependence of the Interlayer Exchange Coupling in Ferromagnetic Multilayers, *Phys. Rev. Lett.* **88**, 167206 (2002).
- [16] N. Persat and A. Dinia, Strong temperature dependence of the interlayer exchange coupling strength in Co/Cu/Co sandwiches, *Phys. Rev. B* **56**, 2676 (1997).
- [17] R. P. Erickson, K. B. Hathaway, and J. R. Cullen, Mechanism for non-Heisenberg-exchange coupling between ferromagnetic layers, *Phys. Rev. B* **47**, 2626 (1993).
- [18] D. M. Edwards, J. Mathon, R. B. Muniz, and M. S. Phan, Oscillations of the Exchange in Magnetic Multilayers as an Analog of de Haas-van Alphen Effect, *Phys. Rev. Lett.* **67**, 493 (1991).
- [19] Z. P. Shi, P. M. Levy, and J. L. Fry, Spin Polarization of Epitaxial Cr on Fe(001) and Interlayer Magnetic Coupling in Fe/Cr Multilayered Structures, *Phys. Rev. Lett.* **69**, 3678 (1992).
- [20] P. Bruno, Theory of interlayer magnetic coupling, *Phys. Rev. B* **52**, 411 (1995).
- [21] Q. L. He, X. Kou, A. J. Grutter, G. Yin, L. Pan, X. Che, Y. Liu, T. Nie, B. Zhang, S. M. Disseler, B. J. Kirby, W. Ratcliff II, Q. Shao, K. Murata, X. Zhu, G. Yu, Y. Fan, M. Montazeri, X. Han, J. A. Borchers, and K. L. Wang, Tailoring exchange couplings in magnetic topological-insulator/antiferromagnetic heterostructures, *Nat. Mater.* **16**, 94 (2016).
- [22] B. B. Chen, H. R. Xu, C. Ma, S. Mattauch, D. Lan, F. Jin, Z. Guo, S. Y. Wan, P. F. Chen, G. Y. Gao, F. Chen, Y. X. Su, and W. B. Wu, All-oxide-based synthetic antiferromagnets exhibiting layer-resolved magnetization reversal, *Science* **357**, 191 (2017).
- [23] A. M. Haghiri-Gosnet and J. P. Renard, CMR manganites: Physics, thin films and devices, *J. Phys. D: Appl. Phys.* **36**, R127 (2003).
- [24] H. R. Xu, S. Y. Wan, B. B. Chen, C. Ma, F. Jin, Z. Guo, D. La, F. Chen, and W. B. Wu, Antiferromagnetic interlayer exchange coupling in all-perovskite  $\text{La}_{0.7}\text{Sr}_{0.3}\text{MnO}_3/\text{SrRu}_{1-x}\text{Ti}_x\text{O}_3$  superlattice, *Appl. Phys. Lett.* **110**, 082402 (2017).
- [25] P. F. Chen, B. B. Chen, X. L. Tan, H. R. Xu, X. F. Xuan, Z. Guo, F. Jin, and W. B. Wu, High- $T_C$  ferromagnetic order in  $\text{CaRuO}_3/\text{La}_{2/3}\text{Ca}_{1/3}\text{MnO}_3$  superlattices, *Appl. Phys. Lett.* **103**, 262402 (2013); B. B. Chen, P. F. Chen, H. R. Xu, X. L. Tan, F. Jin, Z. Guo, B. W. Zhi, and W. B. Wu, Contrasting size-scaling behavior of ferromagnetism in  $\text{La}_{0.67}\text{Ca}_{0.33}\text{MnO}_3$  films and  $\text{La}_{0.67}\text{Ca}_{0.33}\text{MnO}_3/\text{CaRuO}_3$  multilayers, *Appl. Phys. Lett.* **104**, 242416 (2014).
- [26] H. Boschker, J. Verbeeck, R. Egoavil, S. Bals, G. van Tendeloo, M. Huijben, E. P. Houwman, G. Koster, D. H. A. Blank, and G. Rijnders, Preventing the reconstruction of the polar discontinuity at oxide heterointerfaces, *Adv. Funct. Mater.* **22**, 2235 (2012).
- [27] E. J. Moon, P. V. Balachandran, B. J. Kirby, D. J. Keavney, R. J. Sichel-Tissot, C. M. Schlepütz, E. Karapetrova, X. M. Cheng, J. M. Rondinelli, and S. J. May, Effect of interfacial octahedral behavior in ultrathin manganite films, *Nano Lett.* **14**, 2509 (2014).
- [28] M. Ziese and L. Vrejoiu, Properties of manganite/ruthenate superlattice with ultrathin layers, *Phys. Status Solidi RRL.* **7**, 243 (2013); M. Ziese, F. Bern, E. Pipel, D. Hesse, and I. Vrejoiu, Stabilization of ferromagnetic order in  $\text{La}_{0.7}\text{Sr}_{0.3}\text{MnO}_3-\text{SrRuO}_3$  superlattices, *Nano Lett.* **12**, 4276 (2012).
- [29] Z. Huang, K. Han, S. W. Zeng, M. Motapothula, A. Y. Borisovich, S. Ghosh, W. Lü, C. J. Li, W. X. Zhou, Z. Q. Liu, M. Coey, T. Venkatesan, and Ariando, The effect of polar fluctuation and lattice mismatch on carrier mobility at Oxide interfaces, *Nano Lett.* **16**, 2307 (2016).
- [30] T. He and R. J. Cava, Disorder-induced ferromagnetism in  $\text{CaRuO}_3$ , *Phys. Rev. B* **63**, 172403 (2001).
- [31] X. Ke, M. S. Rzchowski, L. J. Belenkay, and C. B. Eom, Positive exchange bias in ferromagnetic  $\text{La}_{0.67}\text{Sr}_{0.33}\text{MnO}_3/\text{SrRuO}_3$  bilayers, *Appl. Phys. Lett.* **84**, 5458 (2004).
- [32] M. Charilaou, C. Bordel, and F. Hellman, Magnetization switching and inverted hysteresis in perpendicular antiferromagnetic superlattices, *Appl. Phys. Lett.* **104**, 212405 (2014).
- [33] J. C. Slonczewski, Origin of biquadratic exchange in magnetic multilayers, *J. Appl. Phys.* **73**, 5957 (1993).
- [34] A. Moser, A. Berger, D. T. Margulies, and E. E. Fullerton, Magnetic Tuning of Biquadratic Exchange Coupling in Magnetic Thin Films, *Phys. Rev. Lett.* **91**, 097203 (2003).
- [35] S. O. Demokritov, Biquadratic interlayer coupling in layered magnetic systems, *J. Phys. D: Appl. Phys.* **31**, 925 (1998).
- [36] X. L. Tan, F. Chen, P. F. Chen, H. R. Xu, B. B. Chen, F. Jin, G. Y. Gao, and W. B. Wu, Anisotropic-strain-relaxation-induced crosshatch morphology in epitaxial  $\text{SrTiO}_3/\text{NdGaO}_3$  thin films, *AIP Adv.* **4**, 107109 (2014).
- [37] A. J. Grutter, A. Vailionis, J. A. Borchers, B. J. Kirby, C. L. Flint, C. He, E. Arenholz, and Y. Suzuki, Interfacial symmetry control of emergent ferromagnetism at the nanoscale, *Nano Lett.* **16**, 5647 (2016).
- [38] J. C. Slonczewski, Fluctuation Mechanism for Biquadratic Exchange Coupling in Magnetic Multilayers, *Phys. Rev. Lett.* **67**, 3172 (1991).
- [39] S. W. Jin, G. Y. Gao, Z. Huang, Z. Z. Yin, X. Zheng, and W. B. Wu, Shear-strain-induced low symmetry phase and domain ordering in epitaxial  $\text{La}_{0.7}\text{Sr}_{0.3}\text{MnO}_3$  thin films, *Appl. Phys. Lett.* **92**, 261901 (2008).
- [40] Z. Celinski, B. Heinrich, J. F. Cochran, W. B. Muir, A. S. Arrott, and J. Kirschner, Growth and Magnetic Studies of

- Lattice Expanded Pd in Ultrathin Fe(001)/Pd(001)/Fe(001) Structure, *Phys. Rev. Lett.* **65**, 1156 (1990).
- [41] S. S. Kalarickal, X. Y. Xu, K. Lenz, W. Kuch, and K. Baberschke, Dominant role of thermal magnon excitation in temperature dependence of interlayer exchange coupling: experimental verification, *Phys. Rev. B* **75**, 224429 (2007).
- [42] N. S. Almeida, D. L. Mills, and M. Teitelman, Temperature Variation of the Inter Film Exchange in Magnetic Multilayers: The Influence of Spin Wave Interactions, *Phys. Rev. Lett.* **75**, 733 (1995).
- [43] A. Tamai, M. P. Allan, J. F. Mercure, W. Meevasana, R. Dunkel, D. H. Lu, R. S. Perry, A. P. Mackenzie, D. J. Singh, Z.-X. Shen, and F. Baumberger, Fermi Surface and van Hove Singularities in the Itinerant Metamagnet  $\text{Sr}_3\text{Ru}_2\text{O}_7$ , *Phys. Rev. Lett.* **101**, 026407 (2008).
- [44] F. Baumberger, N. J. C. Ingle, N. Kikugawa, M. A. Hosain, W. Meevasana, R. S. Perry, K. M. Shen, D. H. Lu, A. Damascelli, A. Rost, A. P. Mackenzie, Z. Hussain, and Z.-X. Shen, Nested Fermi Surface and Electronic Instability in  $\text{Ca}_3\text{Ru}_2\text{O}_7$ , *Phys. Rev. Lett.* **96**, 107601 (2006).
- [45] See Supplemental Material at <http://link.aps.org/supplemental/10.1103/PhysRevApplied.10.024035> for cross-section STEM images and EELS line scans of the LSMO/CRTO superlattice of the form  $[2.8/1.2]_{10}$  grown on NGO(001),  $M$ - $H$  curves of LSMO/CRTO superlattices of the form  $[x/1.2]_{10}$  grown on NGO(001) with different LSMO layer thickness, a schematic crystalline structure and lattice constants of LSMO (pseudocubic), NGO (orthorhombic), and LSAT (cubic), and lattice mismatches for LSMO grown on different substrates.